Monthly Notices
of the
ROYAL ASTRONOMICAL SOCIETY

Mon. Not. R. Astron. Soc. **424,** 3178–3191 (2012) doi:10.1111/j.1365-2966.2012.21496.x

Pre-main-sequence isochrones – I. The Pleiades benchmark

Cameron P. M. Bell,[1⋆] Tim Naylor,[1] N. J. Mayne,[1] R. D. Jeffries[2] and S. P. Littlefair[3]

[1] *School of Physics, University of Exeter, Exeter EX4 4QL*
[2] *Astrophysics Group, Research Institute for the Environment, Physical Sciences and Applied Mathematics, Keele University, Staffordshire ST5 5BG*
[3] *Department of Physics and Astronomy, University of Sheffield, Sheffield S3 7RH*

Accepted 2012 June 11. Received 2012 June 8; in original form 2012 February 10

ABSTRACT

We present a critical assessment of commonly used pre-main-sequence isochrones by comparing their predictions to a set of well-calibrated colour–magnitude diagrams of the Pleiades in the wavelength range 0.4–2.5 μm. Our analysis shows that for temperatures less than 4000 K, the models systematically overestimate the flux by a factor of 2 at 0.5 μm, though this decreases with wavelength, becoming negligible at 2.2 μm. In optical colours this will result in the ages for stars younger than 10 Myr being underestimated by factors of between 2 and 3.

We show that using observations of standard stars to transform the data into a standard system can introduce significant errors in the positioning of pre-main sequences in colour–magnitude diagrams. Therefore, we have compared the models to the data in the natural photometric system in which the observations were taken. Thus we have constructed and tested a model of the system responses for the Wide-Field Camera on the Isaac Newton Telescope.

As a benchmark test for the development of pre-main-sequence models, we provide both our system responses and the Pleiades sequence.

Key words: techniques: photometric – stars: evolution – stars: fundamental parameters – Hertzsprung–Russell and colour–magnitude diagrams – stars: pre-main-sequence – open clusters and associations: general.

1 INTRODUCTION

Our understanding of time-dependent physical processes in young pre-main-sequence (pre-MS) and main-sequence (MS) populations is fundamentally limited by poorly constrained time-scales, the derivation of which requires the determination of ages for pre-MS stellar populations. These ages are generally derived via the comparison of photometric observations of pre-MS stars in young open clusters with theoretical models (or isochrones) using colour–magnitude diagrams (CMDs).

Many previous studies deriving stellar parameters from observations of young clusters in this way have shown large discrepancies between the photometric data and the model predictions. It has been well documented that pre-MS isochrones generally do not fit the entire data set in CMDs; for example, whilst tracing the sequence defined by the higher mass members they will not simultaneously follow the sequence in the lower mass regime (see for instance Hartmann 2003; Stauffer et al. 2007). In addition, pre-MS isochrones from different evolutionary models give ages that differ by a factor of 2 for the same cluster (e.g. Dahm 2005; Mayne et al. 2007). Furthermore, the same data set compared to isochrones in different colours can lead to different age determinations (e.g. Naylor et al. 2002).

The situation has become even more uncertain with the realization that ages derived from the MS are systematically older by a factor of 1.5–2 than ages derived from the pre-MS (e.g. Naylor 2009). To make further progress we require a precise test of the pre-MS models to determine whether the ages could be in error by such a large factor, and if any parts of the pre-MS or any colour combinations are reliable age indicators. Our longer term aim is that if we have a clear understanding of the limitations of pre-MS ages, we may be able to create a reliable pre-MS age scale.

In this work, therefore, we set up a benchmark test for pre-MS isochrones. Most obviously that benchmark must be a cluster that contains a significant number of pre-MS objects, as well as a populated MS to show that the models at least fit these more evolved stars. In addition it should have distance and age determinations which are independent of the CMD, and preferably a low extinction (which might otherwise complicate transformations). Given that most pre-MS isochrones are only available for solar metallicity, the cluster must be at least close to solar composition. Finally, it should be nearby so that the lowest possible masses can be accessed. The Pleiades is the only cluster which fits all these criteria, and Stauffer et al. (2007) have already undertaken a comparison in V and I_c, which shows that at least the V-band luminosity is not matched by two models available at that time.

⋆E-mail: bell@astro.ex.ac.uk

In this paper we return to the Pleiades with the aim of assessing which of the most recent models best match the data. This then allows us to quantify the remaining mismatch so that we can make a realistic assessment of its impact on pre-MS ages. We trace the mismatch as a function of wavelength using observations in a set of filters which are contiguous in wavelength and cover 0.4–2.5 μm. The data reach cooler temperatures than the Stauffer et al. (2007) study, and are free of the uncertainties introduced by transforming heterogeneous data sets into a standard photometric system.

In Section 2 we describe the set of interior and atmospheric theoretical models we have studied and examine systematic differences between the different formalisms. In Section 3 we describe a set of observations, of both standard stars and the Pleiades, which we use to test the models. In Section 4 we compare the models to the Pleiades data set using CMDs. Section 5 describes the comparison of the models to a sample of MS binaries with dynamically constrained masses. In Section 6 we quantify the mismatch between the models and the data as a function of wavelength. Our conclusions are detailed in Section 7.

2 THE MODELS

To derive fundamental parameters, such as age and distance, from fitting CMDs we require model isochrones, which must also be transformed into the requisite photometric system. Isochrones are constructed from stellar interior models that predict $L_{\rm bol}$, $T_{\rm eff}$ and surface gravity ($\log g$). Colours are then calculated through a colour–$T_{\rm eff}$ relation and magnitudes via bolometric corrections to $L_{\rm bol}$. Both relations can be derived by folding atmospheric model flux distributions through the appropriate photometric filter responses. The colours and magnitudes must then be calibrated to a standard scale. Therefore, for this study we have adopted a set of pre-MS interior models and also a collection of atmospheric models with which to derive the required relations.

2.1 Pre-main-sequence interior models

We tested those pre-MS interior models that were publicly available, covered a wide range in stellar mass and had been designed specifically for the investigation of pre-MS evolution. The sets of interior models studied here are those of Baraffe et al. (1998; hereafter BCAH98), Siess, Dufour & Forestini (2000, hereafter SDF00), D'Antona & Mazzitelli (1997, hereafter DAM97) and Dotter et al. (2008, hereafter DCJ08[1]). Note that the recent Pisa models (Tognelli, Prada Moroni & Degl'Innocenti 2011) do not extend to the age of the Pleiades (see Section 4.1) and therefore are not used in this study.

Fig. 1 shows the variation between the different pre-MS evolutionary tracks and the 4.6-Gyr isochrone for a range of masses. There are systematic differences in both the mass tracks, especially at young ages, and location of the MS, particularly for low-mass stars. These differences stem from variations in the treatment of various physical processes in addition to the values of adopted parameters. Most notable are the treatment of convection, the opacity sources and the treatment of the stellar interior/atmosphere boundary (see Hillenbrand & White 2004).

[1] Whilst the DCJ08 models are not specifically designed for studying pre-MS evolution, these mass tracks cover the entire pre-MS phase over a significant mass range.

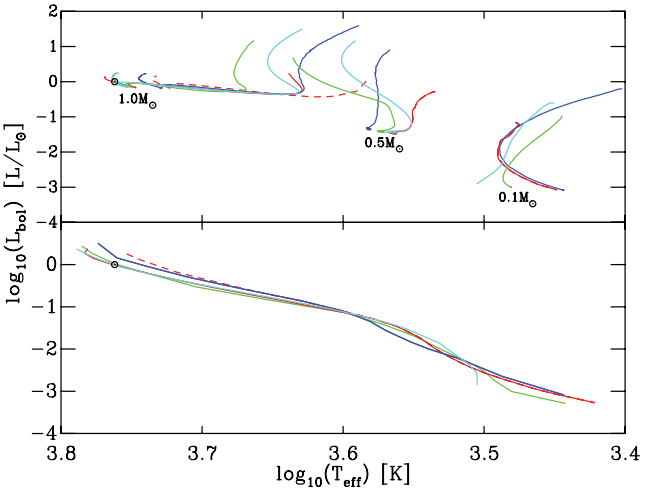

Figure 1. Variation between the pre-MS evolutionary tracks for masses of 0.1, 0.5 and 1.0 $M_\odot$ (top panel) and 4.6-Gyr isochrones (bottom panel) for the following models: BCAH98 $\alpha = 1.9$ (red, continuous), BCAH98 $\alpha = 1.0$ (red, dashed), SDF00 (blue), DAM97 (green) and DCJ08 (cyan). Note that for masses $<0.6\,M_\odot$ both computations of the BCAH98 models are identical; this is due to the insensitivity to the value of the mixing-length parameter in this mass regime.

The BCAH98 models have been computed for two different mixing-length parameters $\alpha = 1.0$ (general mixing-length parameter) and $\alpha = 1.9$ (solar-calibrated value), where for stellar masses below $0.6\,M_\odot$ these models are identical as the dependence on the mixing-length parameter is negligible in this regime (Baraffe et al. 2002). Further, note that the publicly available SDF00 models have a slightly modified solar abundance and mixing-length parameter from the solar-calibrated model (cf. $Z = 0.02$ and $\alpha = 1.5$ with $Z = 0.0249$ and $\alpha = 1.605$ in SDF00).

2.2 Atmospheric models

We required atmospheric model flux distributions to calculate a theoretical colour–$T_{\rm eff}$ relation and bolometric corrections. We produced a spectral library consisting of the PHOENIX BT-Settl model atmospheres for $400 \leq T_{\rm eff} \leq 7800$ K and the ATLAS9 models with newly updated opacity distribution functions (ODFnew) for $8000 \leq T_{\rm eff} \leq 50\,000$ K. Despite the differences in microphysics between the two sets of atmospheric models, we found that at the transitional $T_{\rm eff} = 8000$ K derived colours from both sets of models agree to within 0.02 mag in all colours.

2.2.1 The ATLAS9/ODFnew models

The ATLAS9/ODFnew atmospheric models are those of Castelli & Kurucz (2004).[2] These models are based on the assumption of steady-state plane-parallel layers under the influence of local thermodynamic equilibrium and computed using the solar abundances of Grevesse & Sauval (1998). Line-blanketing effects are computed statistically via the use of the opacity distribution functions which average the contribution from the various atomic and molecular species as described in Kurucz (1979). A pure mixing-length theory (Böhm-Vitense 1958) is used in the computation of these models, and we adopted those termed 'no-overshoot' on the basis that

[2] ftp://ftp.stsci.edu/cdbs/grid/ck04models

these better recreate the observed spectra of stars with $T_{\rm eff}$ greater than the Sun (Castelli, Gratton & Kurucz 1997). The mixing-length parameter is set to $\alpha = 1.25$ with a microturbulent velocity $\xi = 2\,{\rm km\,s^{-1}}$.

2.2.2 *The BT-Settl models*

The BT-Settl atmospheric models are those described in Allard, Homeier & Freytag (2011).[3] These models have been computed using an updated version of the PHOENIX atmospheric code (cf. Allard et al. 2001) to include the updated Barber et al. (2006) BT2 H_2O line list, the revised solar abundances of Asplund et al. (2009) and a sophisticated cloud model that accounts for the settling of dust grains (Allard et al. 2003). The effects of turbulent mixing in the atmosphere are calculated by interpolating from 2D and 3D radiation hydrodynamic models (Ludwig, Allard & Hauschildt 2006), with the treatment of dust for cooler models ($T_{\rm eff} < 2600\,{\rm K}$) based on the dust formation models of Freytag et al. (2010). The effects of opacity are sampled directly using a library of over 700 million lines including atomic and molecular species along the spectrum. The BT-Settl models are computed under the assumption of plane-parallel radiative transfer, where convection is treated using the standard mixing-length theory. The mixing-length parameter is defined to be $\alpha = 2.0$ with a microturbulent velocity of $\xi = 2\,{\rm km\,s^{-1}}$.

3 THE DATA

3.1 Observations

Our observations are a subset of a large survey of pre-MS clusters (the remainder of which will be published in an upcoming paper; Bell et al., in preparation) and were obtained using the 2.5-m Isaac Newton Telescope (INT) on La Palma. The survey was split over two runs, using the same instrumentation and filter set on both occasions, namely the four EEV 2k × 4k CCD Wide-Field Camera (WFC) with a $34 \times 34\,{\rm arcmin^2}$ field of view and the $(UgriZ)_{\rm WFC}$ filter set. A combination of long and short exposures were used to ensure that any bright stars saturated in the longer exposures could be measured in the shorter exposures. Whilst the $(gri)_{\rm WFC}$ filters are based on the Sloan Digital Sky Survey (SDSS) design, there are no similar u and z filters for the WFC, and so the Royal Greenwich Observatory (RGO) $U_{\rm WFC}$ and $Z_{\rm WFC}$ filters were used. The first set of observations were taken during 2007 October 21–26 with the second run during 2008 September 13–19.

Five overlapping fields within the Pleiades open cluster were observed over the course of the two runs (see Fig. 2 and Table 1). In addition, four fields in Stripe 82 of the SDSS were used as standard fields and routinely observed throughout both runs.

3.2 Data reduction

Each image was debiased and flat-fielded using a median stacked bias and flat-field frames. Both the $i_{\rm WFC}$- and $Z_{\rm WFC}$-band images were defringed using library fringe frames. The data were analysed using the CLUSTER package as described in Naylor et al. (2002), Burningham et al. (2003) and Jeffries et al. (2004). The $i_{\rm WFC}$-band images for a particular field were combined (after calculating spatial transformations between separate frames) with the resulting deep image used for object identification and detection. An object list was created and optimal photometry (Naylor 1998) was then

[3] http://www.phoenix.ens-lyon.fr/Grids/BT-Settl/

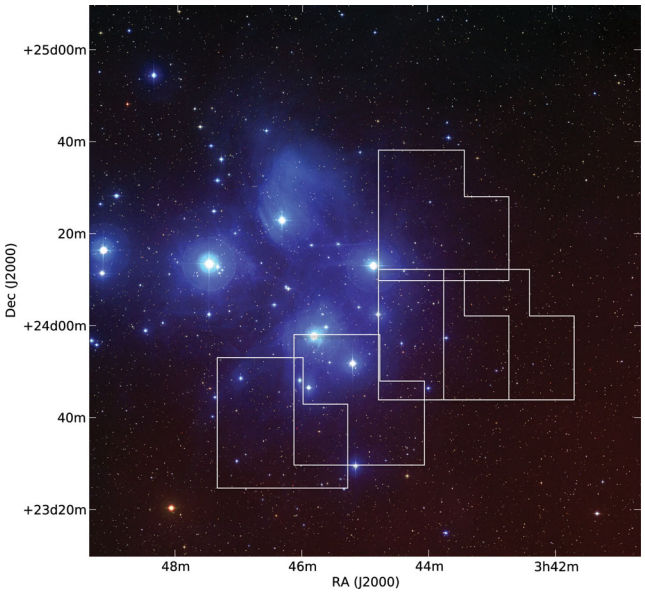

Figure 2. Two square degree three-colour mosaic image of the Pleiades from the ESO Digitized Sky Survey with the five INT-WFC fields of view overlaid. Note that the image is slightly displaced from the central coordinates of $\alpha = 03^{\rm h}47^{\rm m}24^{\rm s}$, $\delta = +24^\circ07'00''$ to illustrate the region chosen to identify low-mass members.

Table 1. The central coordinates for each field of view and exposure times in the INT-WFC bandpasses for the observations of the Pleiades.

Field	RA Dec. (J2000.0)	Filter	Exposure time (s) × 1 unless stated
Pleiades field A	$03^{\rm h}46^{\rm m}19\overset{\rm s}{.}2$ $+23^\circ38'02\overset{''}{.}4$	$U_{\rm WFC}$	1, 10
		$g_{\rm WFC}$	1, 10, 100, 500(× 2)
		$r_{\rm WFC}$	1, 7, 50, 250
		$i_{\rm WFC}$	1, 10, 100(× 2)
		$Z_{\rm WFC}$	1, 7, 50, 250
Pleiades field B	$03^{\rm h}45^{\rm m}00\overset{\rm s}{.}0$ $+23^\circ44'45\overset{''}{.}6$	$U_{\rm WFC}$	1, 10
		$g_{\rm WFC}$	1, 10, 100, 500(× 2)
		$r_{\rm WFC}$	1, 7, 50, 250
		$i_{\rm WFC}$	1, 10, 100(× 2)
		$Z_{\rm WFC}$	1, 7, 50, 250
Pleiades field C	$03^{\rm h}43^{\rm m}44\overset{\rm s}{.}4$ $+23^\circ58'08\overset{''}{.}4$	$U_{\rm WFC}$	1, 10
		$g_{\rm WFC}$	1, 10, 100, 500(× 2)
		$r_{\rm WFC}$	1, 7, 50, 250
		$i_{\rm WFC}$	1, 10, 100(× 2)
		$Z_{\rm WFC}$	1, 7, 50, 250
Pleiades field D	$03^{\rm h}42^{\rm m}36\overset{\rm s}{.}0$ $+23^\circ58'08\overset{''}{.}4$	$U_{\rm WFC}$	1, 10
		$g_{\rm WFC}$	1, 10, 100, 500(× 2)
		$r_{\rm WFC}$	1, 7, 50, 250
		$i_{\rm WFC}$	1, 10, 100(× 2)
		$Z_{\rm WFC}$	1, 7, 50, 250
Pleiades field E	$03^{\rm h}43^{\rm m}44\overset{\rm s}{.}4$ $+24^\circ24'28\overset{''}{.}8$	$U_{\rm WFC}$	1, 10
		$g_{\rm WFC}$	1, 10, 100, 500(× 2)
		$r_{\rm WFC}$	1, 7, 50, 250
		$i_{\rm WFC}$	1, 10, 100(× 2)
		$Z_{\rm WFC}$	1, 7, 50, 250

performed providing a flux for each object at a given position. A spatially varying profile correction was calculated from the bright unsaturated stars in each frame so that the photometry could later be calibrated using standard star observations. Although the $i_{\rm WFC}$-band images were combined, optimal photometry was carried out on each individual frame, so as to ensure that the good signal-to-noise ratio in one frame was not outweighed by a poorer signal-to-noise ratio in another frame upon combining the images. The individual profile corrected measurements of each frame were then combined by weighting each measurement in accordance with its signal-to-noise ratio and accounting for differences in airmass between separate frames. An additional statistical uncertainty was added to each measurement at this stage to ensure that the distribution of chi-squared (χ^2) resulting from combining the measurements versus signal-to-noise ratio was independent of signal-to-noise ratio and of the order of unity (Naylor et al. 2002). The additional statistical uncertainty adopted here ranged from 0.01 from 0.03 mag and reflects uncertainties in the profile correction. Stars with a reduced $\chi^2 > 10$ are generally flagged as variable (see Burningham et al. 2003). For some fields of view, we have combined photometric observations at two different epochs and due to pre-MS variability over such time-scales, there are a number of sources that have thus been flagged. For sources which displayed night-to-night variations, we have replaced the photometry with colours and magnitudes from a single night. The Two Micron All Sky Survey (2MASS; Cutri et al. 2003) was used to provide an astrometric solution for each frame. The rms residual of the six-coefficient fit was approximately 0.2 arcsec.

To create a final optical catalogue of the Pleiades based on the five overlapping fields, it was necessary to combine the individual fields of view. For this process, we used the normalization procedure as described in Jeffries et al. (2004). A running catalogue was created that contained all the derived magnitudes and colours for each object identified in all fields. We then calculated the mean magnitude and colour differences of stars in common between two overlapping fields, and adjusted the zero-points for each field to minimize these differences (in effect allowing for small variations in the zero-point between fields observed on different nights). This process ensures greater consistency between fields in the final catalogue. The resulting zero-point shift is an indicator of the internal consistency of the photometry, as well as the accuracy with which the profile corrections were performed, and suggests an accuracy of $\simeq$1 per cent. Our full Pleiades photometric catalogue is given in Table 2.

3.3 Zero-point stability

Standard field observations were taken on five separate evenings. On only one of the five nights were conditions photometric throughout; the other four nights were affected either at the beginning or at the end by the presence of cloud. We therefore calculated a zero-point for each $g_{\rm WFC}$-band observation by comparing the instrumental magnitudes to those in the SDSS catalogue, and correcting for extinction using a mean $g_{\rm WFC}$-band extinction coefficient ($k_{g_{\rm WFC}} = 0.19$) for La Palma. We could then identify when the zero-point became unstable and define half-nights of bona fide photometric conditions, which were then used for the photometric calibration procedure (the maximum deviation over the course of a single half-night was 0.05 mag). Due to a paucity of blue stars in our standards catalogue, we opted to use the colour range which was most populated [$0.6 \leq (g-i)_{\rm WFC} \leq 1.0$] and define our zero-point at a median colour of $(g-i)_{\rm WFC} = 0.8$. This colour range cut in $(g-i)_{\rm WFC}$ defines the necessary cuts in the other INT-WFC colours [$1.05 \leq (U-g)_{\rm WFC} \leq 1.96$, $0.14 \leq (r-i)_{\rm WFC} \leq 0.31$ and $0.02 \leq (i-Z)_{\rm WFC} \leq 0.18$ with median values of $(U-g)_{\rm WFC} = 1.505$, $(r-i)_{\rm WFC} = 0.225$ and $(i-Z)_{\rm WFC} = 0.1$]. The seeing generally varied between 1 and 2 arcsec in the temporal regions defined above.

3.4 Transforming the data into the standard system

Traditional photometric calibration transforms instrumental magnitudes into magnitudes on a standard system. Typically colours and magnitudes are transformed using linear functions of the form

$$g_{\rm stand} = \psi_g (g-i)_{\rm inst} - k_g \chi + z_g, \quad (1)$$

$$(g-i)_{\rm stand} = \psi_{gi} (g-i)_{\rm inst} - k_{gi} \chi + z_{gi}, \quad (2)$$

where χ is the airmass, k the extinction coefficients, z the zero-points and ψ the colour terms (k, z and ψ are determined from observations of standard stars). Fig. 3 shows the g-band magnitude and $g-i$ colour differences between the standard SDSS and the natural INT-WFC photometric systems (see Appendices A and B, for details). It is immediately obvious that there is no linear colour-dependent transformation that can be applied to INT-WFC observations of MS stars to calibrate them into the standard SDSS photometric system. Even if non-linear MS transformations were created, it is clear that they could not be used to transform observations of red [$(g-i)_{\rm SDSS} \gtrsim 1.8$] pre-MS stars into the standard system. This is due to differences in the spectra between MS and pre-MS stars of the same colour. These differences can result in both g-band magnitude and $g-i$ colour errors of the order of 0.1–0.15 mag at a colour of $(g-i)_{\rm SDSS} \simeq 3$, culminating in stars that ultimately occupy the wrong position in CMD space. Even larger errors can be caused by the difference between the spectrum of a reddened and an unreddened star of the same apparent colour (see Fig. 3). From the calculated SDF00 zero-age main-sequence (ZAMS; see Appendix B) the differential behaviour between MS and pre-MS transformations occurs at an approximate spectral type of between K6 and M0. Mayne et al. (2012) document a similar though more extreme

Table 2. A sample of the full Pleiades photometric catalogue with colours and magnitudes in the natural INT-WFC photometric system. Due to space restrictions, we only show the $g_{\rm WFC}$ and $(g-i)_{\rm WFC}$ colours and magnitudes as a representation of its content. The full photometric catalogue (available as Supporting Information with the online version of the paper) also includes photometry in the $(U-g)_{\rm WFC}$, $(r-i)_{\rm WFC}$ and $(i-Z)_{\rm WFC}$ colours and the $U_{\rm WFC}$, $r_{\rm WFC}$, $i_{\rm WFC}$ and $Z_{\rm WFC}$ magnitudes. Columns list unique identifiers for each star in the catalogue: field and CCD number (integer and decimal), ID, RA and Dec. (J2000.0), CCD pixel coordinates of the star, and for each of $g_{\rm WFC}$ and $(g-i)_{\rm WFC}$ there is a magnitude, an uncertainty on the magnitude and a flag (OO represents a 'clean detection'; see Burningham et al. 2003, for a full description of the flags).

Field	ID	RA (J2000.0)	Dec. (J2000.0)	x	y	$g_{\rm WFC}$	$\sigma_{g_{\rm WFC}}$	Flag	$(g-i)_{\rm WFC}$	$\sigma_{(g-i)_{\rm WFC}}$	Flag
21.04	8	03 46 34.136	+23 37 26.25	1204.056	1439.980	8.236	0.010	OO	−0.412	0.014	OL
22.02	16	03 43 41.521	+23 38 56.30	998.324	2035.800	8.523	0.010	OS	−2.653	0.014	SS

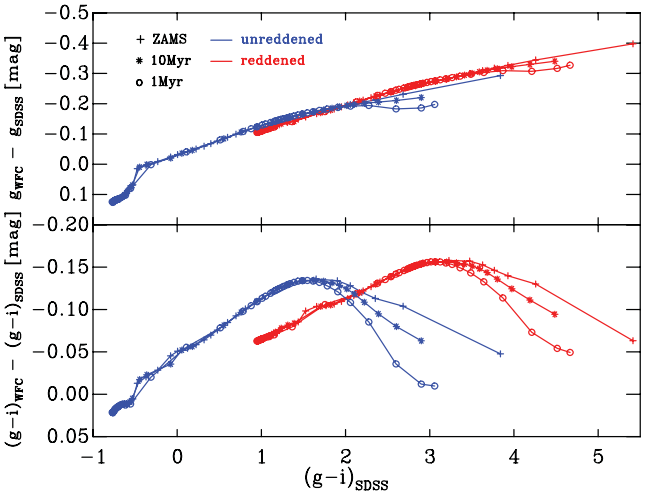

Figure 3. Calculated transformations between the SDSS and INT-WFC photometric systems. The transformations have been calculated for reddened [nominal $E(B-V) = 1$ mag; red] and unreddened (blue) ZAMS (crosses), 10-Myr pre-MS stars (asterisks) and 1-Myr pre-MS stars (open circles). Upper panel: Δg versus $(g-i)_{SDSS}$. Lower panel: $\Delta(g-i)$ versus $(g-i)_{SDSS}$. No single (even non-linear) transformation will calibrate observations of both red [$(g-i)_{SDSS} \gtrsim 1.8$] MS and pre-MS stars into a standard system, and if either are reddened the situation becomes worse [$\simeq$0.15 mag at a colour $(g-i)_{SDSS} \simeq 3$].

situation which can result from using MS transformations for brown dwarfs.

A deviation of up to 0.15 mag may help explain, to some extent, why pre-MS isochrones do not simultaneously fit both the higher and lower mass members within a given cluster (Hartmann 2003; Stauffer et al. 2007; Jeffries et al. 2009), although other factors such as photometric variability, extinction, unresolved binaries, accretion luminosity and poorly constrained opacity line lists in the atmospheric models may also contribute to this (Hartmann 2001; Burningham et al. 2005). Furthermore, this could also have severe implications for cluster age and mass function determinations. Allowing the pre-MS stars in a CMD to 'float' by 0.15 mag in both colour and magnitude can result in an age difference of a factor of 2 through isochrone fitting. The conversion from observable magnitudes and colours into mass estimates are highly age- and model-dependent. Hence, an incorrect age would result in an erroneous mass function estimate, thus making meaningful comparison between cluster mass functions difficult at best.

3.5 Calibrating the natural system

If the observations cannot be transformed into a standard photometric system, then the photometry must remain in the natural photometric system and the theoretical models transformed into this system. To achieve this, we need a reliable model for the throughput for each bandpass as a function of wavelength. We emphasize that this is not simply a matter of using the filter responses, or even multiplying the CCD quantum efficiency by the filter response, but involves allowing for every element from the Earth's atmosphere through to the CCD to create a *system* response. We present our best estimates for the system responses in Appendix A.

Having obtained the system responses it is crucial that we obtain an estimate of how precise these are. In principle, we could achieve this by folding the observed fluxes of spectrophotometric standards through our estimated system responses and seeing how closely the observed and predicted magnitudes match. In practice, such standards have not been measured in sufficient numbers with the range of colours and magnitudes to prove useful for our purposes. Instead, we took a sample of MS stars, used their observed SDSS colours to establish their effective temperatures and then folded model atmospheres of the appropriate temperature through our estimated system responses to find their magnitudes in the INT-WFC system.

We defined our sample of MS stars using a series of colour–colour diagrams to isolate the observed MS in the Stripe 82 fields and trim any obvious outliers. To obtain colours and magnitudes in the INT-WFC system, we then transformed the standard SDSS colours and magnitudes into the INT-WFC photometric system (hereafter WFC_{calc}). These transforms are calculated by folding model atmospheres through both the SDSS and our estimated INT-WFC responses and are given in Table 3. The details of these calculations are given in Appendix B, and the transformed standards in the INT-WFC colours are given in Table 4.

Table 3. The calculated transformations between the SDSS and INT-WFC photometric systems for unreddened MS stars where Δ represents (INT-WFC − SDSS). The full table is available as Supporting Information with the online version of the paper; a sample is shown here as a representation of its content.

T_{eff}	$\log g$	Δg	$\Delta(g-i)$	$(g-i)_{SDSS}$	$\Delta(u-g)$	$(u-g)_{SDSS}$	$\Delta(r-i)$	$(r-i)_{SDSS}$	$\Delta(i-z)$	$(i-z)_{SDSS}$
2775	5.25	−0.293 00	−0.047 65	3.839 61	0.012 64	4.129 61	0.246 88	2.200 01	−0.174 76	1.221 23
3290	5.11	−0.230 94	−0.103 91	2.683 86	−0.025 63	3.064 19	0.128 98	1.208 09	−0.087 04	0.668 67
3528	4.98	−0.212 37	−0.112 99	2.353 55	−0.033 58	2.874 77	0.097 64	0.948 87	−0.067 07	0.531 08
3683	4.92	−0.204 28	−0.120 31	2.193 44	−0.035 95	2.837 17	0.079 40	0.815 97	−0.055 50	0.456 15
3829	4.87	−0.197 61	−0.128 06	2.056 53	−0.037 51	2.819 37	0.061 88	0.701 41	−0.044 29	0.388 59

Table 4. A sample of the transformed Stripe 82 standard star catalogue with colours and magnitudes in the natural INT-WFC photometric system. The full photometric catalogue (available as Supporting Information with the online version of the paper) also includes photometry in the $(U-g)_{WFC}$, $(r-i)_{WFC}$ and $(i-Z)_{WFC}$ colours. Columns list unique identifiers for each star in the catalogue (see Table 2) for details.

Field	ID	RA (J2000.0)	Dec. (J2000.0)	x	y	g_{WFC}	$\sigma_{g_{WFC}}$	Flag	$(g-i)_{WFC}$	$\sigma_{(g-i)_{WFC}}$	Flag
0.00	67737	20 47 07.346	−01 05 52.53	0.000	0.000	17.158	0.006	OO	0.585	0.008	OO
0.00	67740	20 47 09.412	−01 04 17.09	0.000	0.000	14.721	0.006	OO	0.482	0.008	OO

With the INT-WFC standards established, we can evaluate how well constrained the calculated system responses of the INT-WFC are. Calculating zero-points in the colour ranges specified in Section 3.3 and applying these zero-points and extinction coefficients only (no colour terms) to all standard field observations, we created a set of observed standard star colours and magnitudes in the INT-WFC system. To create a single catalogue for each of the four standard fields, we performed the normalization process as described in Section 3.2 and merged all four fields to create a catalogue of observed colours and magnitudes of Stripe 82 standards in the INT-WFC photometric system (hereafter $\mathrm{WFC_{obs}}$). After the normalization procedure, we examined, for each star, the magnitude shift between each observation and the mean observed magnitude. This is an indicator of the internal precision of our photometry, and we found that $g_{\mathrm{rms}} = 0.011$ mag, $(g-i)_{\mathrm{rms}} = 0.014$ mag, $(U-g)_{\mathrm{rms}} = 0.020$ mag, $(r-i)_{\mathrm{rms}} = 0.011$ mag and $(i-Z)_{\mathrm{rms}} = 0.010$ mag. We attribute the slightly poorer precision in U_{WFC} to a lack of colour-dependent atmospheric extinction terms.

The differences $\mathrm{WFC_{calc}} - \mathrm{WFC_{obs}}$ are shown in Figs 4–8. Using bin sizes of 0.25 mag in colour, and only data with uncertainties of less than 0.03 mag, we calculated the median value in each colour bin as an indicator of the level of agreement between the $\mathrm{WFC_{calc}}$ and $\mathrm{WFC_{obs}}$ catalogues in a given colour range. A paucity of data at extreme colours forced us to relax our restrictions on the uncertainty in the data points to less than 0.1 mag, and where the number of stars was insufficient to calculate the median value in a given colour bin (taken as five), the individual data points were plotted. These plots show that we reproduce the zero-point to within 0.01 mag at the colours which we defined to calculate the zero-points in Section 3.3. The remaining residuals lie within the ± 0.02 mag level across the entire colour range except for a small region in the U_{WFC} band and colours redder than $(g-i)_{\mathrm{WFC}} \simeq 2$ in the i_{WFC} band.

The most obvious causes of any disagreement between $\mathrm{WFC_{calc}}$ and $\mathrm{WFC_{obs}}$ are that our estimated system responses are incorrect and that the atmospheric models are incorrect. In an attempt

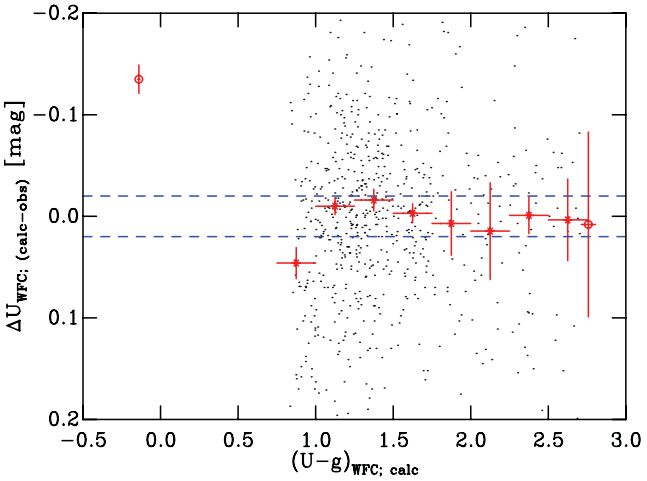

Figure 4. Magnitude difference in the U_{WFC} band between the $\mathrm{WFC_{calc}}$ and $\mathrm{WFC_{obs}}$ photometric catalogues as a function of $(U-g)_{\mathrm{WFC;calc}}$. Asterisks represent the median value of all points in a given bin of size 0.25 mag in colour. The error bars on these symbols are the standard error about the median value. Open circles represent individual data points and are plotted where the number of points is insufficient to calculate the median value in a given bin (defined as five). The error bars of these symbols are the individual uncertainties associated with that point. The dashed lines represents the ± 0.02 mag level with respect to zero.

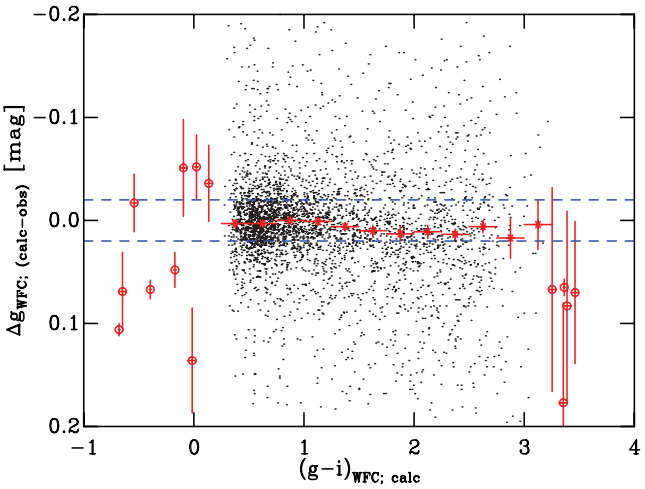

Figure 5. Same as Fig. 4, but for the difference in the g_{WFC} and as a function of $(g-i)_{\mathrm{WFC;calc}}$.

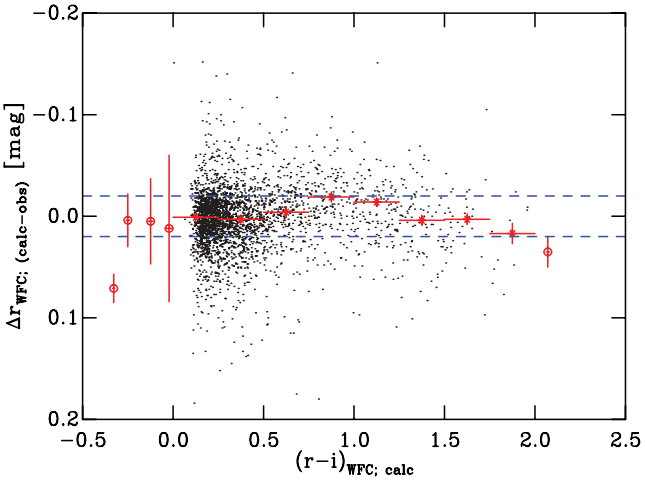

Figure 6. Same as Fig. 4, but for the difference in the r_{WFC} band as a function of $(r-i)_{\mathrm{WFC;calc}}$.

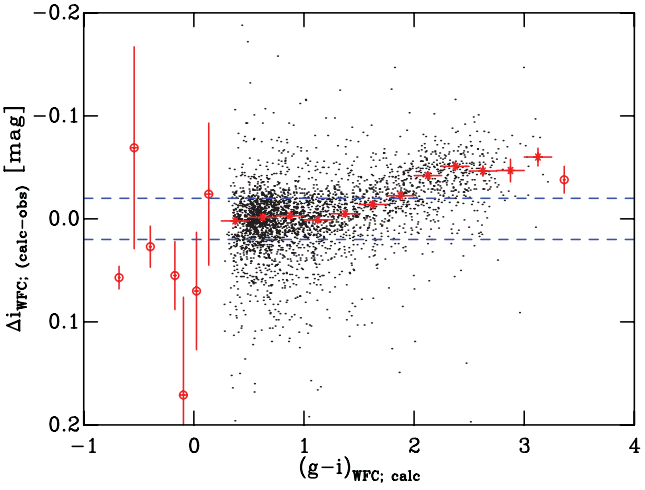

Figure 7. Same as Fig. 4, but for the difference in the i_{WFC} band as a function of $(g-i)_{\mathrm{WFC;calc}}$.

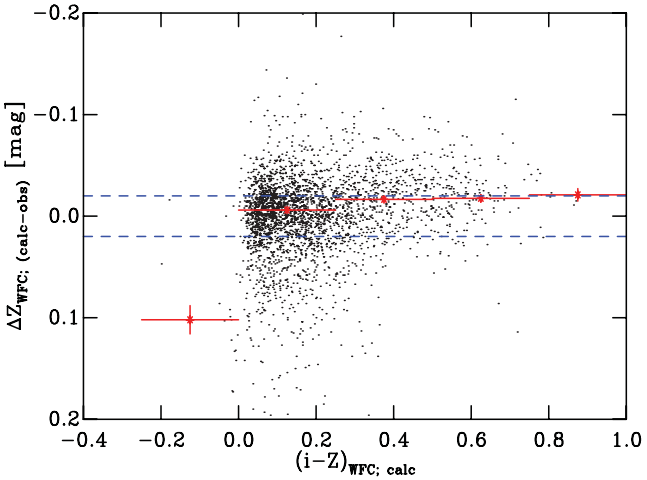

Figure 8. Same as Fig. 4, but for the difference in the $Z_{\rm WFC}$ band as a function of $(i - Z)_{\rm WFC;calc}$.

to obtain some idea of the likely magnitude of the latter effect, we tried recalculating the transforms using different model atmospheres (the PHOENIX/*GAIA* models of Brott & Hauschildt 2005) and the observed spectral library of Pickles (1998). We found these changed the transformations by up to 0.02 mag, nicely explaining the majority of the residuals. It remains unclear whether the remaining residuals are due to errors in the atmospheric fluxes or poorly modelled $U_{\rm WFC}$- and $i_{\rm WFC}$-band system responses. As a result, we retain the system responses in their current calculated form for the remainder of this study, and note the fact there are uncertainties at the levels shown in Figs 4–8.

4 COMPARING THE MODELS AND THE DATA – THE PLEIADES

Having characterized the natural INT-WFC photometric system and calculated the corresponding system responses, we can now test the pre-MS interior and stellar atmospheric models by comparing them to our Pleiades data. We obtained a list of approximately 180 members by cross-correlating our full catalogue with the combined membership catalogues of Stauffer et al. (2007) and Lodieu, Deacon & Hambly (2012). This membership list is given in Table 5.

4.1 Model parameters

We used a distance modulus dm = 5.63 which is based on the trigonometric parallax of Soderblom et al. (2005). We chose to rely on the lithium depletion age, since although it is based on the predictions of stellar interior models, Jeffries & Oliveira (2005) show there is a very high level of agreement between the various models. Furthermore, we used the age based on the boundary in $K_{\rm s}$ (130 Myr) of Barrado y Navascués, Stauffer & Jayawardhana (2004), since, as we shall show later, $K_{\rm s}$ is the best predictor of luminosity available to us. We used a reddening of $E(B - V) = 0.04$ based on the mean extinction $A_V = 0.12$ (see Stauffer et al. 1998) and $R_V = 3.2$. Hence, to transform the theoretical models into the observable plane, we first reddened the atmospheric models by a nominal $E(B - V) = 0.04$ using the reddening law of Cardelli, Clayton & Mathis (1989) and then calculated bolometric corrections using equation (B2).

4.2 Discussion

Fig. 9 shows four CMDs of the Pleiades with the pre-MS isochrones of BCAH98, SDF00, DAM97 and DCJ08 overlaid. The break between MS and pre-MS stars in the Pleiades occurs at $(g - i)_{\rm WFC} \simeq 2$, and is marked by a paucity of stars in all CMDs. It is clear that the isochrones all follow the Pleiades MS reasonably well, though as we shall see in Section 6 this is in part is due to compensating errors in each individual band. None of the models, however, traces the observed pre-MS locus, with each predicting colours that are too blue for a given stellar mass. This issue has already been highlighted by Stauffer et al. (2007; see their fig. 13), though from their data one could only be certain there was a problem in the V band, whereas our data show that all optical bands are affected.

This is part of a broader picture where it is known that MS stars are similarly affected, at least in the V band (see Section 5). It is well known that there are sources of opacity missing from the atmospheric models for cool stars ($T_{\rm eff} \lesssim 3700$ K) in the optical regime of the spectrum (Leggett et al. 1996; Alvarez & Plez 1998; BCAH98; Baraffe et al. 2002). Although the BT-Settl models are computed using more complete line lists than previous generations of PHOENIX models, there is still a need for additional data to provide fully comprehensive line lists, especially for the molecular opacities (H_2O, TiO, CH_4, etc.; see Partridge & Schwenke 1997; Schwenke 1998).

If we are to be quantitative about the missing opacity, we need to measure the missing flux individually in each bandpass, rather than as a function of colour. The most straightforward way of achieving this is to identify a photometric bandpass where the missing sources of opacity are minimal, and create colours with respect to that band. This is equivalent to using the luminosity in that band to define the temperature. To test the temperature scale requires masses (from which the models predict temperatures) from binaries, data which are simply not available for the Pleiades. Instead, as the opacity problem affects MS stars as well as pre-MS stars (in the same $T_{\rm eff}$ range), we will use MS binaries to identify a band we can use.

5 COMPARING THE MODELS AND THE DATA – MAIN-SEQUENCE BINARIES

Although there are many MS binaries with well-determined masses and distances we could use to test the models, the outstanding problem is the small subsample of these which have individual magnitudes in many colours. Astrometric binaries are often separated in the infrared (IR) and so lack individual optical colours, and

Table 5. A sample of the catalogue of colours and magnitudes in the natural INT-WFC photometric system for Pleiades members. The columns and content are in the same format as Table 2. The full photometric catalogue is available as Supporting Information with the online version of the paper.

Field	ID	RA (J2000.0)	Dec. (J2000.0)	x	y	$g_{\rm WFC}$	$\sigma_{g_{\rm WFC}}$	Flag	$(g - i)_{\rm WFC}$	$\sigma_{(g-i)_{\rm WFC}}$	Flag
24.02	45	03 41 03.006	+23 43 21.42	426.717	3696.221	17.653	0.006	OO	2.553	0.006	OO
24.02	118	03 41 05.230	+23 50 14.82	526.182	2444.212	20.400	0.015	OO	3.228	0.017	OO

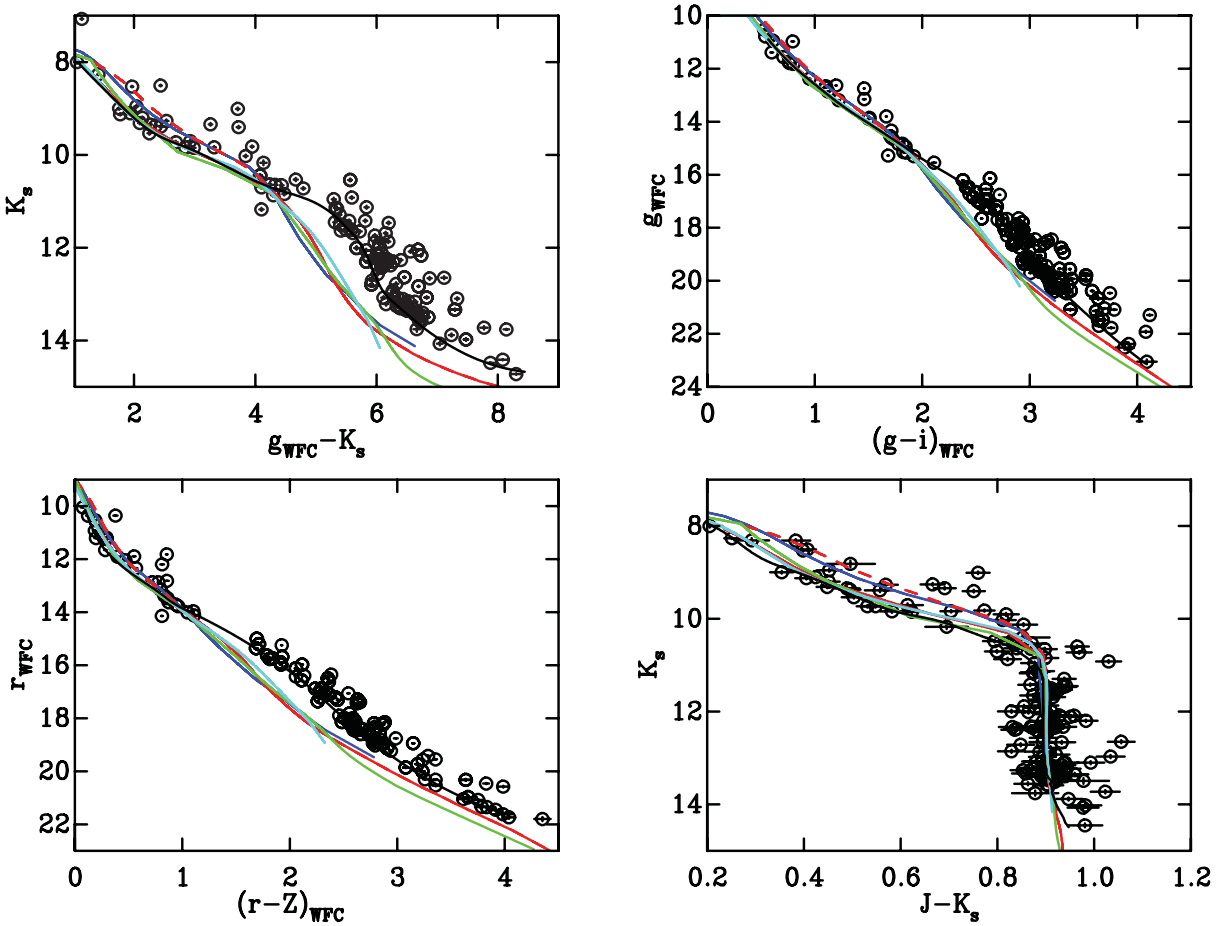

Figure 9. Optical/near-IR CMDs of Pleiades members. The 130-Myr pre-MS isochrones of BCAH98 $\alpha = 1.9$ (red, continuous), BCAH98 $\alpha = 1.0$ (red, dashed), SDF00 (blue), DAM97 (green) and DCJ08 (cyan) are overlaid, adopting a distance modulus d$m = 5.63$ and a reddening $E(B - V) = 0.04$. The isochrones have been transformed into the observable plane using bolometric corrections derived by folding the atmospheric model flux distributions (see Section 2.2) through the calculated INT-WFC system responses. The black line in each panel represents the spline fit (by eye) to the Pleiades single-star sequence. The open circles represent the photometric data, with the associated uncertainties in colour and magnitude shown as the bars. Top left: K_s, $g_{WFC} - K_s$ CMD. Top right: g_{WFC}, $(g - i)_{WFC}$ CMD. Bottom left: r_{WFC}, $(i - Z)_{WFC}$ CMD. Bottom right: K_s, $J - K_s$ CMD.

eclipsing binaries often have light curves in only a small number of colours. To overcome this problem, we will model the system magnitude, which as we shall discuss later still gives significant insight as a function of stellar temperature.

5.1 The sample

To create our sample, data for low-mass binaries from Delfosse et al. (2000) were supplemented with data for higher mass binaries from Andersen et al. (1987), Clausen et al. (2008, 2009), Clement et al. (1997a,b), Lacy et al. (1997, 2005), López-Morales & Ribas (2005), Popper et al. (1986), Popper (1994, 1997), Torres et al. (1997) and Torres, Sandberg Lacy & Claret (2009). We imposed an upper limit to the mass uncertainty on both the primary and secondary components of 10 per cent, and in addition limited ourselves to non-contact binaries in which the effects of tidal forces and mass transfer may bias the results. We also limited the sample to binaries with associated uncertainties in the parallax of $\leq$11 per cent; thus our conclusions are unaffected by the Lutz–Kelker bias (Lutz & Kelker 1973). The sample spans the mass range $0.1 \leq M_{\odot} \leq 1.4$ for the individual components, with the higher mass limit chosen as the BCAH98 models only extend to such masses. For the low-mass systems in Delfosse et al. (2000), the apparent magnitudes were from the homogeneous data set of Leggett (1992). A number of higher mass systems only had a Strömgren $b - y$ colour, and so these were transformed into $V - I_c$ colours according to the relation of Bessell (1979) which is accurate to within 0.01 mag for MS stars. Near-IR measurements were taken from the 2MASS point source catalogue (Cutri et al. 2003). Parallax measurements were taken from the *Hipparcos* catalogue (Perryman et al. 1997), the Yale General Catalogue of Trigonometric Stellar Parallaxes (van Altena, Lee & Hoffleit 1995) and Ségransan et al. (2000).

5.2 The models

We adopted 2-Gyr isochrones with which to compare observations against theory as we expect these binaries, which are located in the field, to be old systems. Note that at such ages, the mass scale is insensitive to changes in age. For each binary component, the bolometric luminosity (L_{bol}), defined by the stellar interior models, was converted into an absolute magnitude using bolometric corrections calculated using equation (B2) by folding the atmospheric models through the revised *UBVRI* responses of Bessell & Murphy (2012) and the *JHK*$_s$ responses of Cohen et al. (2003). For the reference

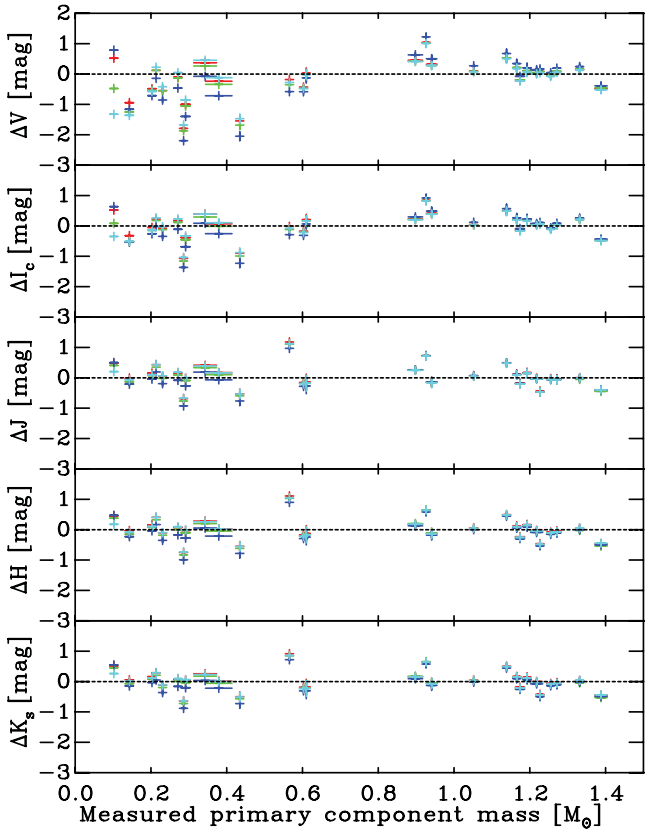

Figure 10. The difference between the observed and theoretically predicted system absolute magnitudes (where Δ implies calculated − observed) for the 28 binary systems as a function of the measured primary component stellar mass. Bolometric luminosities have been calculated using 2-Gyr interior models of BCAH98 $\alpha = 1.9$ (red), SDF00 (blue), DAM97 (green) and DCJ08 (cyan). The atmospheric model flux distribution were folded through the revised *UBVRI* responses of Bessell & Murphy (2012) and the JHK_s responses of Cohen, Wheaton & Megeath (2003) to create bolometric corrections which were used to derive the predicted absolute magnitudes. Upper panel: ΔV. Upper middle panel: ΔI_c. Middle panel: ΔJ. Lower middle panel: ΔH. Lower panel: ΔK_s.

Vega spectrum we used the CALSPEC alpha_lyr_stis_005[4] spectrum with $V = 0.03$ and all colours equal to zero. For the 2MASS responses, we used the bandpass specific reference spectra and zero-point offsets of Cohen et al. (2003; see their table 2 and section 5, respectively). The absolute magnitude was then converted into a flux, and the fluxes for a given binary pair were then summed and converted back into an absolute system magnitude. Where possible, we have included the effects of interstellar reddening by adopting literature values. These values range from $E(B-V) = 0.0$ to 0.11. The atmospheric models were reddened accordingly and the bolometric corrections calculated as discussed in Section 4.1.

5.3 Discussion

Fig. 10 shows the residuals (calculated − observed) in luminosity relation in different bandpasses. As the binary mass ratio $q \rightarrow 1$ both components have the same mass, whereas when $q \rightarrow 0$ the primary component is likely to dominate the flux output of the system. Thus we plot the difference in absolute magnitude as a function of the measured primary mass. The range of q as defined by our sample is $q = m_2/m_1 = 0.33$–1.0, where for 65 per cent of these the ratio $q > 0.9$. Regardless of the choice of interior model, there are significant systematic deviations (especially in the optical regime) for masses below $\simeq$0.4–0.5 $M_\odot$. Fig. 10 shows that the differences between the observed and calculated system absolute magnitude decrease as one moves to redder bandpasses, from approximately 2.5 mag in the V band to less than 1 mag in the K_s band. In the near-IR, and in particular the K_s band, there is far less spread for a given stellar mass (see also Martín et al. 2000 and Delfosse et al. 2000), with the interior models predicting similar luminosities. This further highlights the fact that there is a problem with the optical colours predicted by the atmospheric models for masses below $\simeq$ 0.4–0.5 $M_\odot$ ($T_{\rm eff} \lesssim 3700$ K).

It has been noted in the literature that short-period, close-in binary system components have radii which are inflated of the order of 10 per cent with respect to evolutionary models of low-mass MS stars (e.g. Kraus et al. 2011). To test whether we observe this effect in the photometry of these systems, we plotted Fig. 10 as a function of physical separation. We found no evidence for the models to either underpredict or overpredict the absolute system magnitude for short-period binaries with smaller physical separations.

What is clear, however, is that of all the bands available, the K_s-band magnitude is closest to that predicted by the models for a given temperature, both in terms of mean magnitude and spread. This is unsurprising, since the K_s band is less affected than either the J or H band by the missing sources of opacity that arise from incomplete H_2O line lists (see the discussion on the completeness of the BT2 H_2O line list as a function of wavelength by Barber et al. 2006). In what follows, therefore, we will use the K_s-band magnitude to determine the temperatures of Pleiades members.

6 QUANTIFYING THE DISCREPANCY

Our approach for quantifying the effects of the missing opacity is to determine the temperature of a given Pleiad by comparing its K_s-band magnitude with that predicted by a given model. We can then compare the predicted luminosity in any other band with that of the member in question to calculate the missing flux. In practice, it is better to work with a sequence than individual members, and so we defined the single-star Pleiades sequence in the INT-WFC and 2MASS colours by fitting a spline (by eye) to the observed sequence in various CMDs. We used only stars with uncertainties in both colour and magnitude of less than 0.1 mag. This spline lies slightly above the lower envelope of the sequence to account for photometric uncertainties and takes into consideration that the equal-mass binary sequence lies $\simeq$0.75 mag above the single-star sequence (with very few systems of higher multiplicity). Table 6 provides the single-star sequence in the $(griZ)_{\rm WFC}JHK_s$ bandpasses.

Starting, for instance, with the K_s, $(g_{\rm WFC} - K_s)$ Pleiades CMD, we compared the theoretical 130-Myr isochrone to the observed spline and thus calculated the difference between the colours at a given $T_{\rm eff}$ (provided by the model isochrone). Assuming that the problem, in this case, lies in the $g_{\rm WFC}$ band and not in K_s, this then defines the required correction (ΔBC; defined as $\rm BC_{obs} - BC_{calc}$) for the $g_{\rm WFC}$ band at a specific $T_{\rm eff}$. This process was then repeated over the $T_{\rm eff}$ range of the theoretical isochrone or the colour range specified by the observed spline, whichever was more restrictive, thus providing ΔBC as a function of $T_{\rm eff}$ for the $g_{\rm WFC}$ band. Repeating this for all four pre-MS evolutionary models (including both the BCAH98 computations), we calculated the model-dependent ΔBCs as a function of $T_{\rm eff}$ for the $(griZ)_{\rm WFC}JH$ bandpasses.

[4] http://www.stsci.edu/hst/observatory/cdbs/calspec.html

Table 6. The Pleiades single-star sequence in the INT-WFC and 2MASS bandpasses. The full table is available as Supporting Information with the online version of the paper; a sample is shown here as a representation of its content.

$g_{\rm WFC}$	$r_{\rm WFC}$	$i_{\rm WFC}$	$Z_{\rm WFC}$	J	H	$K_{\rm s}$
10.807	10.377	10.270	10.251	9.370	9.082	8.987
10.972	10.505	10.389	10.364	9.484	9.181	9.078
11.133	10.645	10.516	10.481	9.594	9.275	9.166
11.292	10.783	10.640	10.596	9.699	9.364	9.251
11.445	10.914	10.758	10.704	9.796	9.445	9.330
11.593	11.040	10.871	10.809	9.887	9.520	9.405
11.735	11.161	10.979	10.908	9.970	9.588	9.473
11.870	11.273	11.079	11.000	10.043	9.646	9.534
11.998	11.378	11.172	11.086	10.110	9.699	9.589
12.120	11.478	11.261	11.168	10.169	9.745	9.637

Our final results are shown in Fig. 11. In the Pleiades, stars cooler than $T_{\rm eff} \simeq 4000$ K are on the pre-MS, and all models fail to match the data in the optical in this regime. The discrepancy is large, 0.75 mag in $g_{\rm WFC}$, but decreases with increasing wavelength. This is a clear improvement over the PHOENIX/*GAIA* models, for which we find a discrepancy of around 1 mag.

We can test what effect the overestimation in flux of the atmospheric models has on the derived ages for $T_{\rm eff} < 4000$ K in the following way. If this discrepancy is independent of age (and therefore $\log g$), the roughly logarithmic age spacing between the isochrones in CMD space means that the resulting error in age is best represented as a fractional rather than an absolute difference. We begin by taking the BCAH98 $\alpha = 1.9$ isochrones and adding our ΔBCs derived above to the theoretical bolometric corrections and colour–$T_{\rm eff}$ relations at a given age. We then find the closest matching uncorrected BCAH98 $\alpha = 1.9$ isochrone (in CMD space). Comparing these, we find that for ages between 3 and 10 Myr, the difference in age is approximately a factor of 3 in g, $g - i$ and 2 in r, $r - z$.

The message here is very clear: one should use the reddest waveband possible to determine an age. Unfortunately, by the time one reaches the $JHK_{\rm s}$ bandpasses, the pre-MS isochrones are vertical with a colour $J - K_{\rm s} \simeq 0.85$ for $2500 < T_{\rm eff} < 4000$ K. Although individual stars descend with age, the resulting sequences are almost degenerate with age, and for young clusters (<10 Myr), observations are further complicated by the presence of discs. Thus the $JHK_{\rm s}$ IR is unlikely to yield reliable young cluster ages. Masses do not suffer from such a degeneracy and therefore the H band may be a reliable mass indicator when $K_{\rm s}$ is affected by circumstellar material.

Perhaps more surprising is the fact that in the MS regime, hotter than $T_{\rm eff} \simeq 4000$ K, only two models fit the data in the optical. The reason the BCAH98 $\alpha = 1.0$ and SDF00 models tend to overpredict the luminosity at a given $T_{\rm eff}$ is that neither is tuned to the Sun, as

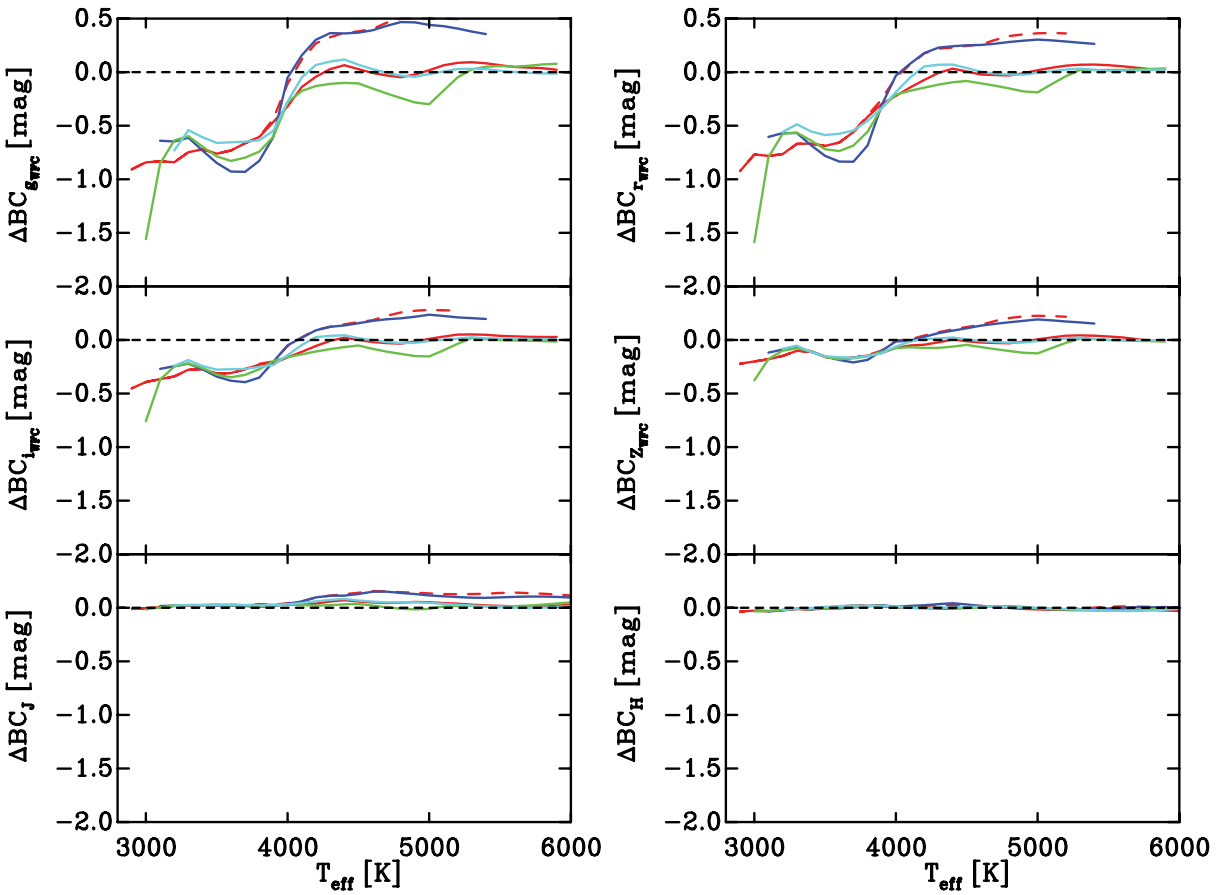

Figure 11. Model-dependent corrections (ΔBC) calculated as a function of $T_{\rm eff}$ for the optical $(griZ)_{\rm WFC}$ and near-IR JH bandpasses. The corrections were calculated as the difference between the theoretically predicted colour and the observed colour of the Pleiades sequence at a given $T_{\rm eff}$. Corrections have been calculated for the following models: BCAH98 $\alpha = 1.9$ (red, continuous), BCAH98 $\alpha = 1.0$ (red, dashed), SDF00 (blue), DAM97 (green) and DCJ08 (cyan). For $T_{\rm eff} \lesssim 4000$ K all the models fail to match the data in the optical regime, with the magnitude of the mismatch decreasing with increasing wavelength.

explained in Section 2.1. Once the BCAH98 models have a tuned mixing-length paramater ($\alpha = 1.9$) based on matching observed solar values they are a good match to the MS data. A possible reason why the DAM97 models fail to fit the MS may be because of their treatment of convection.

7 CONCLUSIONS

We have carried out a precise test of a set of pre-MS models by examining how well they match the Pleiades sequence in optical and near-IR CMDs. The stages we have gone through to achieve this are as follows.

(i) We have demonstrated that traditional photometric calibration, using observations of standard stars to transform the data into a standard photometric system, should not be used for studies of pre-MS stars. Differences in $\log g$ and $T_{\rm eff}$ between a MS star and a pre-MS star of the same colour can, for instance, result in errors of the order of 0.1–0.15 mag in both the g-band magnitude and $g - i$ colour for red stars. Hence, it is crucial that precise photometric studies (especially of pre-MS objects) be carried out in the natural photometric system of the observations.

(ii) Therefore, we have calculated system responses for the natural INT-WFC photometric system. Our observations show these are a good model of the photometric system.

(iii) We have demonstrated that for all optical colours, no pre-MS model follows the observed Pleiades sequence for temperatures cooler than 4000 K. The models overestimate the flux by a factor of 2 at 0.5 μm, with the difference decreasing with increasing wavelength. We believe there is little observable effect at 2.2 μm, as the $K_{\rm s}$-band magnitude of MS binaries matches the models at this wavelength.

(iv) These differences in bolometric correction correspond to underestimating the ages of pre-MS stars younger than 10 Myr by factors of 2–3, depending on the choice of colours used. Thus the errors in pre-MS isochrone models can explain the discrepancy between MS and pre-MS ages found by Naylor (2009), and imply the ages determined from the MS are more likely to be correct.

(v) We have provided both our system responses and our Pleiades sequence in such a way that it can be used as a benchmark for any new evolutionary models. These are given in Tables A1 and 6, respectively, and will also be made available from the Cluster Collaboration home page[5] and the CDS archive.

ACKNOWLEDGMENTS

CPMB is funded by a UK Science and Technology Facilities Council (STFC) studentship. SPL is supported by an RCUK fellowship. This research has made use of data obtained at the Isaac Newton Telescope which is operated on the island of La Palma by the Isaac Newton Group (ING) in the Spanish Observatorio del Roque de los Muchachos of the Institutio de Astrofisica de Canarias. This research has made use of archival data products from the Two Micron All Sky Survey (2MASS), which is a joint project of the University of Massachusetts and the Infrared Processing and Analysis Center, funded by the National Aeronautics and Space Administration (NASA) and the National Science Foundation. The authors would like to thank the referee for comments which significantly improved the structure of the paper.

[5] http://www.astro.ex.ac.uk/people/timn/Catalogues/

REFERENCES

Allard F., Hauschildt P. H., Alexander D. R., Tamanai A., Schweitzer A., 2001, ApJ, 556, 357
Allard F., Guillot T., Ludwig H.-G., Hauschildt P. H., Schweitzer A., Alexander D. R., Ferguson J. W., 2003, in Martín E., ed., Proc. IAU Symp. 211, Brown Dwarfs, p. 325
Allard F., Homeier D., Freytag B., 2011, in Johns-Krull C., Browning M. K., West A. A., eds, ASP Conf. Ser. Vol. 448, Motel Atmospheres From Very Low Mass Stars to Brown Dwarfs. Astron. Soc. Pac., San Francisco, p. 91
Allen C. W., 1963, in Allen C. W., ed., Astrophysical Quantities. Athlone Press, The Univ. of London, London
Alvarez R., Plez B., 1998, A&A, 330, 1109
Andersen J., Nordstrom B., Garcia J. M., Gimenez A., 1987, A&A, 174, 107
Asplund M., Grevesse N., Sauval A. J., Scott P., 2009, ARA&A, 47, 481
Baraffe I., Chabrier G., Allard F., Hauschildt P. H., 1998, A&A, 337, 403 (BCAH98)
Baraffe I., Chabrier G., Allard F., Hauschildt P. H., 2002, A&A, 382, 563
Barber R. J., Tennyson J., Harris G. J., Tolchenov R. N., 2006, MNRAS, 368, 1087
Barrado y Navascués D., Stauffer J. R., Jayawardhana R., 2004, ApJ, 614, 386
Bessell M. S., 1979, PASP, 91, 589
Bessell M. S., 1990, PASP, 102, 1181
Bessell M., Murphy S., 2012, PASP, 124, 140
Bessell M. S., Castelli F., Plez B., 1998, A&A, 333, 231
Böhm-Vitense E., 1958, Z. Astrophys., 46, 108
Brott I., Hauschildt P. H., 2005, in Turon C., O'Flaherty K. S., Perryman M. A. C., eds, ESA SP-576, The Three-Dimensional Universe with Gaia, p. 565
Burningham B., Naylor T., Jeffries R. D., Devey C. R., 2003, MNRAS, 346, 1143
Burningham B., Naylor T., Littlefair S. P., Jeffries R. D., 2005, MNRAS, 363, 1389
Cardelli J. A., Clayton G. C., Mathis J. S., 1989, ApJ, 345, 245
Castelli F., Kurucz R. L., 2004, preprint (astro-ph/0405087)
Castelli F., Gratton R. G., Kurucz R. L., 1997, A&A, 318, 841
Cavadore C., Dorn R. J., 2000, in Amico P., Beletic J. W., eds, Astrophysics and Space Science Library, Vol. 252, Optical Detectors for Astronom II. Kluwer, Dordrecht, p. 25
Clausen J. V., Torres G., Bruntt H., Andersen J., Nordström B., Stefanik R. P., Latham D. W., Southworth J., 2008, A&A, 487, 1095
Clausen J. V., Bruntt H., Claret A., Larsen A., Andersen J., Nordström B., Giménez A., 2009, A&A, 502, 253
Clement R., Reglero V., Garcia M., Fabregat J., Suso J., 1997a, A&AS, 124, 499
Clement R., Garcia M., Reglero V., Suso J., Fabregat J., 1997b, A&AS, 125, 529
Cohen M., Wheaton W. A., Megeath S. T., 2003, AJ, 126, 1090
Cutri R. M. et al., 2003, 2MASS Point Source Catalogue (available at http://www.ipac.caltech.edu/2mass/)
Dahm S. E., 2005, AJ, 130, 1805
D'Antona F., Mazzitelli I., 1997, Mem. Soc. Astron. Ital., 68, 807 (DAM97)
Delfosse X., Forveille T., Ségransan D., Beuzit J., Udry S., Perrier C., Mayor M., 2000, A&A, 364, 217
Doi M. et al., 2010, AJ, 139, 1628
Dotter A., Chaboyer B., Jevremović D., Kostov V., Baron E., Ferguson J. W., 2008, ApJS, 178, 89 (DCJ08)
Freytag B., Allard F., Ludwig H.-G., Homeier D., Steffen M., 2010, A&A, 513, A19
Fukugita M., Ichikawa T., Gunn J. E., Doi M., Shimasaku K., Schneider D. P., 1996, AJ, 111, 1748
Girardi L., Bertelli G., Bressan A., Chiosi C., Groenewegen M. A. T., Marigo P., Salasnich B., Weiss A., 2002, A&A, 391, 195
Grevesse N., Sauval A. J., 1998, Space Sci. Rev., 85, 161
Hartmann L., 2001, AJ, 121, 1030

Hartmann L., 2003, ApJ, 585, 398
Hillenbrand L. A., White R. J., 2004, ApJ, 604, 741
Jeffries R. D., Oliveira J. M., 2005, MNRAS, 358, 13
Jeffries R. D., Naylor T., Devey C. R., Totten E. J., 2004, MNRAS, 351, 1401
Jeffries R. D., Naylor T., Walter F. M., Pozzo M. P., Devey C. R., 2009, MNRAS, 393, 538
King D. L., 1985, RGO/La Palma Technical Note, 31, 1
Kraus A. L., Tucker R. A., Thompson M. I., Craine E. R., Hillenbrand L. A., 2011, ApJ, 728, 48
Kurucz R. L., 1979, ApJS, 40, 1
Kurucz R. L., 1992, in Barbuy B., Renzini A., eds, Proc. IAU Symp. 149, The Stellar Populations of Galaxies. Kluwer, Dordrecht, p. 225
Lacy C. H. S., Torres G., Latham D. W., Zakirov M. M., Arzumanyants G. C., 1997, AJ, 114, 1206
Lacy C. H. S., Torres G., Claret A., Vaz L. P. R., 2005, AJ, 130, 2838
Leggett S. K., 1992, ApJS, 82, 351
Leggett S. K., Allard F., Berriman G., Dahn C. C., Hauschildt P. H., 1996, ApJS, 104, 117
Lodieu N., Deacon N. R., Hambly N. C., 2012, MNRAS, 422, 1495
López-Morales M., Ribas I., 2005, ApJ, 631, 1120
Ludwig H.-G., Allard F., Hauschildt P. H., 2006, A&A, 459, 599
Lutz T. E., Kelker D. H., 1973, PASP, 85, 573
Martín E. L., Brandner W., Bouvier J., Luhman K. L., Stauffer J., Basri G., Zapatero Osorio M. R., Barrado y Navascués D., 2000, ApJ, 543, 299
Mayne N. J., Naylor T., Littlefair S. P., Saunders E. S., Jeffries R. D., 2007, MNRAS, 375, 1220
Mayne N. J., Harries T. J., Rowe J., Acreman D. M., 2012, MNRAS, 3011
Naylor T., 1998, MNRAS, 296, 339
Naylor T., 2009, MNRAS, 399, 432
Naylor T., Totten E. J., Jeffries R. D., Pozzo M., Devey C. R., Thompson S. A., 2002, MNRAS, 335, 291
Oke J. B., Gunn J. E., 1983, ApJ, 266, 713
Partridge H., Schwenke D. W., 1997, J. Chem. Phys., 106, 4618
Perryman M. A. C. et al., 1997, A&A, 323, L49
Pickles A. J., 1998, PASP, 110, 863
Popper D. M., 1994, AJ, 108, 1091
Popper D. M., 1997, AJ, 113, 1457
Popper D. M., Lacy C. H., Frueh M. L., Turner A. E., 1986, AJ, 91, 383
Schwenke D. W., 1998, Faraday Discussions, 109, 321
Ségransan D., Delfosse X., Forveille T., Beuzit J., Udry S., Perrier C., Mayor M., 2000, A&A, 364, 665
Shahbaz T., Smale A. P., Naylor T., Charles P. A., van Paradijs J., Hassall B. J. M., Callanan P., 1996, MNRAS, 282, 1437
Siess L., Dufour E., Forestini M., 2000, A&A, 358, 593 (SDF00)
Soderblom D. R., Nelan E., Benedict G. F., McArthur B., Ramirez I., Spiesman W., Jones B. F., 2005, AJ, 129, 1616
Stauffer J. R., Schild R., Barrado y Navascués D., Backman D. E., Angelova A. M., Kirkpatrick J. D., Hambly N., Vanzi L., 1998, ApJ, 504, 805
Stauffer J. R. et al., 2007, ApJS, 172, 663
Tognelli E., Prada Moroni P. G., Degl'Innocenti S., 2011, A&A, 533, A109
Torres G., Stefanik R. P., Andersen J., Nordstrom B., Latham D. W., Clausen J. V., 1997, AJ, 114, 2764
Torres G., Sandberg Lacy C. H., Claret A., 2009, AJ, 138, 1622
van Altena W. F., Lee J. T., Hoffleit E. D., 1995, in van Altena W. F., Lee J. T., Hoffleit E. D., eds, The General Catalogue of Trigonometric Stellar Parallaxes, 4th edn. Yale University Observatory, New Haven
Verbeek K. et al., 2012, MNRAS, 420, 1115

APPENDIX A: THE CALCULATED INT-WFC SYSTEM RESPONSES

Although the SDSS survey system responses are well constrained and available on the SDSS web pages[6] (Doi et al. 2010), the responses on the Isaac Newton Group (ING) web pages for the WFC only combine the filter throughput and CCD quantum efficiency. To model the system responses of the INT-WFC, we included the cumulative effects of the transmission of the Earth's atmosphere, the reflectivity of the telescope mirror, the transmission of the prime focus corrector optics, the quantum efficiency of the detector and the filter transmission. To calculate the atmospheric transmission we used the model for the La Palma atmosphere derived by King (1985), for an airmass typical for our observations of 1.4. This model varies smoothly as a function of wavelength and does not include the molecular absorption features. These atmospheric absorption bands (primarily due to H_2O, CO_2 and O_3) were estimated using the spectrum of an F8 star observed using the Faint Object Spectrograph on the William Herschel Telescope. At low resolution the continuum of an F8 star is relatively smooth, and thus the atmospheric bands can be identified by fitting a low-order polynomial to the continuum and subtracting this from the spectrum (Shahbaz et al. 1996). The continuum is modelled between 4700 and 9800 Å. At prime focus the INT optical path involves a single reflection from the aluminium-coated primary mirror, and this was modelled using the aluminium reflectivity spectrum of Allen (1963). A three-element prime focus corrector is used, which is coated to minimize reflection and thus improve efficiency and reduce ghosts. The first two elements are non-interchangeable and have a broad-band single-layer MgF_2 coating. The third element, although interchangeable, typically adds an additional single layer of MgF_2 coating. These single-layer coatings produce total reflectivities smaller than 2 per cent in the wavelength region 3500–7400 Å. Beyond this range, the reflectivity from the prime focus corrector increases to $\simeq$3 per cent at 8000 Å. The filter and detector responses were from the ING web pages.[7] The detector is comprised of four EEV42-80 CCDs. The detector response on the ING web pages only extends to 3400 Å in the blue; however, the blue edge of the RGO $U_{\rm WFC}$ filter is at approximately 3000 Å and so the detector response was extended

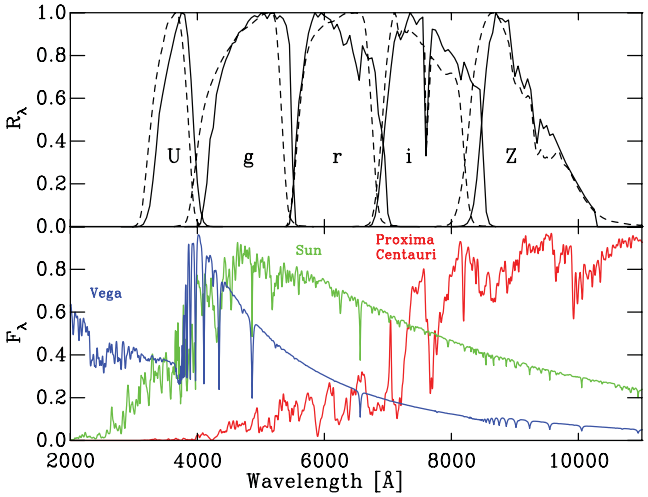

Figure A1. The normalized system response functions for the SDSS (dashed) and the INT-WFC (bold). The INT-WFC system responses are those calculated in Appendix A and include the effects of the telescope optics and atmospheric absorption. Plotted in the bottom panel are normalized model spectra of Vega (A0V), the Sun (G2V) and Proxima Centauri (M6V).

[6] http://www.sdss.org/dr7/instruments/imager/index.html#filters

[7] http://www.ing.iac.es/Astronomy/instruments/wfc/

Table A1. The normalized calculated INT-WFC system responses.

λ	U_{WFC}	λ	g_{WFC}	λ	r_{WFC}	λ	i_{WFC}	λ	Z_{WFC}
3050	0.000	4000	0.000	5400	0.000	6700	0.000	8050	0.000
3100	0.002	4050	0.015	5450	0.013	6750	0.010	8100	0.001
3150	0.011	4100	0.099	5500	0.142	6800	0.050	8150	0.002
3200	0.042	4150	0.203	5550	0.384	6850	0.142	8200	0.005
3250	0.097	4200	0.409	5600	0.586	6900	0.285	8250	0.015
3300	0.216	4250	0.463	5650	0.684	6950	0.462	8300	0.041
3350	0.356	4300	0.618	5700	0.812	7000	0.605	8350	0.104
3400	0.528	4350	0.676	5750	0.904	7050	0.745	8400	0.223
3450	0.614	4400	0.736	5800	0.957	7100	0.863	8450	0.391
3500	0.694	4450	0.781	5850	1.000	7150	0.915	8500	0.570
3550	0.767	4500	0.813	5900	0.980	7200	0.873	8550	0.736
3600	0.832	4550	0.855	5950	0.998	7250	0.906	8600	0.861
3650	0.902	4600	0.864	6000	0.986	7300	0.956	8650	0.906
3700	0.954	4650	0.905	6050	0.976	7350	1.000	8700	1.000
3750	1.000	4700	0.918	6100	0.966	7400	0.978	8750	0.974
3800	0.992	4750	0.930	6150	0.923	7450	0.945	8800	0.971
3850	0.885	4800	0.959	6200	0.946	7500	0.968	8850	0.956
3900	0.684	4850	0.976	6250	0.909	7550	0.980	8900	0.966
3950	0.425	4900	0.986	6300	0.848	7600	0.331	8950	0.829
4000	0.206	4950	0.979	6350	0.856	7650	0.736	9000	0.702
4050	0.074	5000	0.996	6400	0.894	7700	0.923	9050	0.751
4100	0.021	5050	0.998	6450	0.817	7750	0.919	9100	0.687
4150	0.005	5100	0.972	6500	0.758	7800	0.889	9150	0.645
4200	0.001	5150	0.997	6550	0.684	7850	0.848	9200	0.691
4250	0.000	5200	1.000	6600	0.845	7900	0.819	9250	0.640
		5250	0.970	6650	0.809	7950	0.828	9300	0.493
		5300	0.985	6700	0.784	8000	0.809	9350	0.390
		5350	0.972	6750	0.789	8050	0.789	9400	0.502
		5400	0.939	6800	0.721	8100	0.759	9450	0.458
		5450	0.851	6850	0.526	8150	0.686	9500	0.473
		5500	0.285	6900	0.455	8200	0.769	9550	0.426
		5550	0.011	6950	0.329	8250	0.731	9600	0.433
		5600	0.000	7000	0.061	8300	0.686	9650	0.400
				7050	0.008	8350	0.660	9700	0.366
				7100	0.003	8400	0.652	9750	0.333
				7150	0.001	8450	0.641	9800	0.299
				7200	0.000	8500	0.341	9850	0.272
						8550	0.068	9900	0.245
						8600	0.013	9950	0.219
						8650	0.003	10 000	0.192
						8700	0.000	10 050	0.167
								10 100	0.141
								10 150	0.119
								10 200	0.097
								10 250	0.080
								10 300	0.000

bluewards using data for an almost identical EEV44-82 CCD to a wavelength of 3200 Å and further extrapolated to 3000 Å (Cavadore & Dorn 2000). The RGO Z_{WFC} filter response data become noisy at wavelengths greater than 9000 Å, and so this response was extended redwards using calculated 4-mm Schott RG850 data to $\simeq$10 300 Å where the detector response approaches zero. Any negative values for the filter responses from the ING web pages were removed. Note also that the RGO U_{WFC} filter response used here does not include the recently discovered red leak near 7050 Å (Verbeek et al. 2012). The calculated INT-WFC system responses are shown in the top panel of Fig. A1, with the individual bandpass throughputs given in Table A1.

APPENDIX B: CALCULATING THE THEORETICAL TRANSFORMATIONS

To investigate what effect variations in the system responses between the standard SDSS and natural INT-WFC photometric systems would have on the calibration of our photometric data, we calculated the magnitude and colour differences between the two photometric systems. We adopted the standard SDSS responses and the calculated INT-WFC responses, and folded the atmospheric models through both. For this comparison we were interested only in the relative differences in the derived colours and magnitudes, and so our conclusions are not be affected by the use of atmospheric models.

Following the formalism of Girardi et al. (2002), a synthetic apparent magnitude m_{R_λ} in a given filter with response function R_λ is calculated as

$$m_{R_\lambda} = -2.5 \log \left(\frac{\int_\lambda \lambda f_\lambda R_\lambda \mathrm{d}\lambda}{\int_\lambda \lambda f_\lambda^\circ R_\lambda \mathrm{d}\lambda} \right) + m_{R_\lambda}^\circ, \quad \text{(B1)}$$

where f_λ is the stellar flux as observed at Earth and f_λ° denotes a reference spectrum with a known apparent magnitude $m_{R_\lambda}^\circ$. The response function R_λ is the product of the component responses described in Appendix A. Note that the integrands in equation (B1) imply photon counting across the filter which is appropriate for detectors such as CCDs.

Stellar atmospheric models only contain information about the flux at the stellar surface, F_λ. The transformation from f_λ to F_λ requires knowledge of the stellar radius, its distance and an extinction curve A_λ to account for interstellar extinction. To incorporate these and remove the radial dependence, it is more convenient to deal in terms of bolometric corrections, which can be formulated as

$$\mathrm{BC}_{R_\lambda} = \mathrm{M}_{\mathrm{bol},\odot} - 2.5 \log \left(\frac{4\pi (10\,\mathrm{pc})^2 F_{\mathrm{bol}}}{\mathrm{L}_\odot} \right) + 2.5 \log \left(\frac{\int_\lambda \lambda F_\lambda 10^{-0.4 A_\lambda} R_\lambda \, \mathrm{d}\lambda}{\int_\lambda \lambda f_\lambda^\circ R_\lambda \, \mathrm{d}\lambda} \right) - m_{R_\lambda}^\circ, \quad \text{(B2)}$$

where $F_{\mathrm{bol}} = \sigma T_{\mathrm{eff}}^4$ is the total flux emergent at the stellar surface and all other symbols retain their original definitions. For the solar values we used $\mathrm{M}_{\mathrm{bol},\odot} = 4.74$ and $\mathrm{L}_\odot = 3.855 \times 10^{33}\,\mathrm{erg\,s^{-1}}$ (Bessell, Castelli & Plez 1998).

The SDSS photometric system is based on a monochromatic AB magnitude system (see Oke & Gunn 1983; Fukugita et al. 1996) which by definition means that a reference spectrum of constant flux density per unit frequency f_ν° will have AB magnitudes $m_\nu^\circ = 0$ at all frequencies ν. By converting this reference spectrum in equation (B2) to energy per unit wavelength according to $f_\lambda = c/\lambda^2 f_\nu$, this definition can then be extended to any photometric system with the result that $m_\lambda^\circ = 0$ are the reference magnitudes. Thus the magnitude and colour differences for a given flux distribution between the INT-WFC and SDSS photometric systems were then simply calculated as the difference in the derived bolometric corrections.

We required bolometric corrections for the MS and pre-MS regimes. To model the changing T_{eff} and $\log g$ values along the MS (from $\log g \simeq 4$ for early B-type stars to $\simeq$5.5 for late M-type stars), we used the calculated ZAMS of SDF00 for stellar masses in the range 0.1–7 $\mathrm{M}_\odot$. For the pre-MS values we adopted the SDF00 interior models for ages of 1 and 10 Myr, calculating T_{eff} and $\log g$ over the same mass range. The reason for choosing the SDF00 interior models over other pre-MS stellar interior models was simply because they span a greater range of stellar masses and so more thoroughly map the MS. Due to the degree of model dependency in pre-MS evolutionary models, we repeated the calculation of the theoretical transformations using the ZAMS T_{eff}, $\log g$ values from the BCAH98, DAM97 and DCJ08 models and found that all four sets of evolutionary models agree to within 0.02 mag over the range of stellar masses.

Fig. 3 shows the calculated magnitude and colour differences for reddened and unreddened objects [for illustrative purposes, we adopted a nominal reddening of $E(B-V) = 1$]. The simple formalism adopted in the derivation of the bolometric corrections allowed us to include the effects of interstellar reddening by applying a given extinction curve A_λ and calculating the bolometric correction as shown in equation (B2). We adopted the Cardelli et al. (1989) extinction curve of $R_V = A_V/E(B-V)$ and thus derived the extinction in a given bandpass at a specific $E(B-V)$. We adopted $R_V = 3.2$ as this value best reproduced the colour-dependent reddening vector of Bessell et al. (1998) upon folding the ATLAS9 'no-overshoot' atmospheric models (Kurucz 1992) through the *UBVRI* responses of Bessell (1990). Magnitude and colour differences were calculated for each T_{eff}, $\log g$ combination in both the MS and pre-MS regimes via linear interpolation.

SUPPORTING INFORMATION

Additional Supporting Information may be found in the online version of this article:

Table 2. The full Pleiades photometric catalogue with colours and magnitudes in the natural INT-WFC photometric system.
Table 3. The calculated transformations between the SDSS and INT-WFC photometric systems for unreddened MS stars where Δ represents (INT-WFC − SDSS).
Table 4. The transformed Stripe 82 standard star catalogue with colours and magnitudes in the natural INT-WFC photometric system.
Table 5. The catalogue of colours and magnitudes in the natural INT-WFC photometric system for Pleiades members.
Table 6. The Pleiades single-star sequence in the INT-WFC and 2MASS bandpasses.

Please note: Wiley-Blackwell are not responsible for the content or functionality of any supporting materials supplied by the authors. Any queries (other than missing material) should be directed to the corresponding author for the article.

This paper has been typeset from a TEX/LATEX file prepared by the author.